Contents list available at CBIORE journal website

International Journal of Renewable Energy Development

Journal homepage: https://ijred.cbiore.id

Research Article

Effect of generator temperature on steam ejector performance in renewable refrigeration cycle considering wet steam model and dry steam model

Jian Jiang and Yanping Yin *

Guangxi Technological College of Machinery and Electricity, Nanning 530007, China

Abstract. The rise in global warming has led to an increased utilization of cooling systems. High energy consumption associated with common refrigeration cycles not only contributes to air pollution but also intensifies the consumption of fossil fuels. Consequently, the imperative to conserve energy has become paramount in today's world. One of the methods to decrease energy consumption involves employing systems capable of harnessing waste heat from industries, solar energy, and other sources. The ejector refrigeration cycle (ERC) stands as an example of such systems. In present study, the impact of elevating the generator temperature on various aspects such as flow behavior in the ejector, aerodynamic shocks, entrainment ratio (ER), and entropy production was examined. The investigation encompassed both wet steam model (WSM) and dry steam model (DSM). Based on the findings, it was observed that with an increase in generator temperature, the ER decreases while the production entropy increases. In the WSM, the liquid mass fraction (LMF) also experiences an increase. Additionally, the Mach number distribution in the DSM surpasses that of the WSM and the temperature drop in the DSM is greater compared to the WSM. With the rise in generator temperature from 388 K to 418 K, both the DSM and WSM exhibit a decrease in ER by 52.9% and 58.7%, respectively. Furthermore, the production entropy experiences a substantial increase of 180% and 206% for the DSM and WSM, respectively.

Keywords: Ejector refrigeration cycle, Steam Ejector, Generator temperature, Entrainment ratio, Entropy generation.

Received: 4th November 2023; Revised: 14th February 2024; Accepted: 13th March 2024; Available online: 20th March 2024

1. Introduction

Vapor-compression refrigeration systems are widely recognized as the prevailing choice for air conditioning in residential and commercial buildings (Elsheniti *et al.*, 2023; Kulkarni *et al.*, 2023; Yıldız *et al.*, 2023). These systems rely on electrical energy consumption to generate the desired cooling effect, necessitating the use of mechanical compressors for their operation (Alami *et al.*, 2023; H. Zhang *et al.*, 2023). Consequently, the production of greenhouse gases increases due to the emissions associated with electricity generation processes. Air conditioning systems have emerged as significant contributors to greenhouse gas emissions, making them a prominent source of environmental concern. One of the drawbacks associated with refrigeration systems is the utilization of refrigerants that contribute to global warming and ozone layer depletion (Bordbar *et al.*, 2023; Prabakaran et al., 2023; Sharif *et al.*, 2023). In an effort to mitigate electricity consumption in compression refrigeration cycles, alternative refrigeration cycles have been proposed that operate based on thermal energy (Mungyeko Bisulandu *et al.*, 2023). The proposed refrigeration cycles are designed to operate within the temperature range of 90 °C to 130 °C. This thermal energy can be derived from renewable energy sources or harnessed from waste heat generated by industrial processes (Aliabadi, Zhang, *et al.*, 2021; Chen *et al.*, 2023; Liang *et al.*, 2023; Ma *et al.*, 2024; Marenco-Porto *et al.*, 2023; Z. Zhang *et al.*, 2023). Consequently, there is no longer a reliance on electricity consumption to achieve the desired cooling effect. This approach contributes to a reduction in the greenhouse effect.

In recent years, the ERC has garnered significant attention as a thermal start-up refrigeration cycle. At the heart of this cycle lies a crucial component known as the ejector, which plays a pivotal role in initiating the system. (Sarkar *et al.*, 2010) focused on optimizing a simple compression refrigeration cycle that utilized N_2O as the refrigerant. The optimization was conducted based on the output pressure of the compressor. The research examined the impact of various factors such as superheating, internal heat exchanger, and expansion turbine on the overall performance of the system. Additionally, the study investigated how these parameters influenced the system performance when carbon dioxide was used as the refrigerant. The findings revealed that the refrigeration cycle employing N_2O as the refrigerant exhibited a higher performance factor. Interestingly, at the point of maximum performance factor, the compressor pressure ratio reached its minimum value. Sarkar *et al.* and Bhattacharya conducted optimization studies involving two refrigerants, CO_2 and N_2O, in various heating and cooling devices, aiming to enhance their efficiency.(Dokandari *et al.*, 2014) presented a liquid ERC utilizing a CO2-NH3 refrigerant. The researchers applied both the first and second laws of

* Corresponding author
Email: 15878513963@163.com (Y. Yin)

https://doi.org/10.61435/ijred.2024.59394
ISSN: 2252-4940/© 2024.The Author(s). Published by CBIORE

thermodynamics to assess the performance of this novel cycle. Furthermore, the study investigated the impact of using different refrigerants on the overall performance of the ERC.

(Deng *et al*., 2007) conducted an evaluation of the ERC utilizing carbon dioxide as the working fluid. The researchers investigated the relationship between the ER and the steam quality at the ejector outlet. The results indicated that as the output pressure of the compressor increased, the ER from the ejector also increased. However, it was observed that the quality of the steam output from the compressor decreased. In another study, (Lee *et al*., 2006) examined the impact of intermediate condenser temperature on reducing exergy losses and enhancing cycle performance in a simple water cycle utilizing a CO2-NH3 refrigerant. Furthermore, (Yari *et al*., 2011) introduced a new capability of refrigeration cycles by proposing a subcritical refrigeration cycle that combined an ejector with a subcritical CO2 cycle.

Due to the intricate nature of simulating the flow inside the ejector, computational fluid dynamics (CFD) was employed by researchers to investigate the flow behavior. (Banasiak *et al*., 2014) conducted a numerical analysis to determine the irreversibility within the ejector, specifically focusing on the R744 working fluid. The mass flow rate of the mixer was found to have a significant impact on the ejector efficiency, prompting an evaluation of the effects of mixer diameter and length on production entropy. The results demonstrated that both parameters had considerable effects. By reducing the mixer length by 33.3% and increasing the cross-sectional area of the mixer by 17.4%, the overall entropy growth rate increased by 8.9% and 5.4%, respectively. In another study, (Sierra-Pallares *et al*., 2016) performed an entropy generation analysis on an R134a ejector, considering three different mixing chambers. The researchers calculated the local entropy generation and explored how it contributed to reducing irreversibility in different areas of the ejector, specifically in relation to geometrical changes. The results indicated that viscous losses accounted for over 75% of the entropy production.

(Haghparast *et al*., 2018) indicated that the efficiency of the ERC can be enhanced through the precise design of ejectors and a thorough geometric analysis of the system. The researchers conducted both numerical and experimental evaluations to determine the optimal operating conditions and geometrical dimensions of the ejector. The results demonstrated that the ERC exhibited its highest efficiency when operating at the critical point and with the maximum pressure ratio. At these conditions, the ejector experienced minimal exergy losses. The study also highlighted the significant influence of the initial nozzle diameter on the ejector's behavior. Increasing the diameter of the primary nozzle resulted in an overall improvement in the ejector's efficiency. Furthermore, the analysis revealed that the fixed area, the mixing chamber, and the primary nozzle were the locations where the highest exergy losses occurred within the ejector system. These findings emphasize the importance of designing ejectors with precise geometries and optimizing their operating conditions to enhance the overall efficiency and performance of the ERC.

(Besagni *et al*., 2017) pointed out that the ERC could not be expanded in the market, because it has a low performance factor. The ejector has a significant effect on the efficiency of the ERC. The efficiency of ejector systems can be improved by understanding fluid dynamics phenomena. There is still no agreement on the choice of turbulence model in the ejector simulation. It can be seen that the model of k-ω SST performs better than other turbulence models in predicting flow behavior in different ejector geometries. (Mazzelli *et al*., 2015) used numerical and experimental analysis to evaluate common computational techniques in the simulation of air ejectors in supersonic mode. Four turbulence models (k–ε, k–ε realizable, k–ω SST, and the stress–ω Reynolds Stress Model) are considered for two-dimensional and three-dimensional simulation of the ejector, and concluded that there is little difference between turbulence models. In predicting basic parameters such as ER; And the k-ω SST model has a more accurate prediction than other models. Also, epsilon-based models make accurate predictions if the stimulus pressure is small. A good prediction was observed by 2D and 3D models in design conditions. But only the 3D model can make an acceptable prediction in conditions of off-design.

(Abbady *et al*., 2023) reported that operating conditions and geometry have a significant effect on ejector efficiency. Therefore, geometrical parameters should be optimized to achieve optimal performance. But it is not possible to introduce optimal geometric parameters considering different operating conditions. As a result, an ejector is proposed whose geometric parameters can be changed and has a variable geometry. Nozzle exit position (NXP) is one of the variable components of this ejector. If the initial temperature is less than the optimum, the NXP value is equal to zero, and if the initial temperature is equal to or greater than the optimum temperature, the NXP value is considered negative.

Nowadays, researchers have paid much attention to consider the phase change process in the ejector. According to the results of the experiments, the phase change process is observed in the ejector (Tang *et al*., 2019) and numerical methods showed that considering the phase change process has a considerable impact on the simulation results (G. Zhang et al., 2019). (Hui *et al*., 2023) did an energy analysis and exergy analysis of a supersonic nozzle by considering phase change, and investigated the effect of increasing nozzle inlet temperature on inlet flow rate and exergy degradation. (G. Zhang, Wang, Dykas, *et al*., 2022) studied the impact of injecting salt particles on phase change and indicated that salt particles have a considerable effect on condensation in nozzle.

(G. Zhang, Wang, Pourranjbar, *et al*., 2022) suggested that superheating steam from low-grade energy can be a significant technique to increase ejector efficiency. The effect of two-phase heat transfer is investigated on the ER. Two models of dry and wet steam are used and investigated the effect of superheating the incoming steam. It can be seen that the intensity of aerodynamic shocks, phase change and two-phase heat transfer decreases with the increase of superheat degree, and the ER in the dry steam model approaches the WSM. The effect of generator temperature on WSM and DSM is one of the research gaps in the field of two-phase ejectors. Present study has investigated the impact of generator temperature on fluid flow behavior and condensation and evaporation processes and attempts to provide a correct understanding of WSM and DSM. Then, the effect of the generator temperature on the ER is investigated in each of the mentioned models.

(G. Zhang, Wang, Pourranjbar, *et al*., 2022) proposed that utilizing superheated steam from low-grade energy sources could significantly enhance ejector efficiency. The research focused on examining the influence of two-phase heat transfer on the ER. WSM and DSM were employed to investigate the effect of superheating the incoming steam. The findings revealed that with an increase in superheat degree, the intensity of aerodynamic shocks, phase change, and two-phase heat transfer diminished. Additionally, the ER in the DSM approached that of the WSM. Notably, the impact of generator temperature on the WSM and dry DSM remains an area of research gap in the field of two-phase ejectors. Present study aimed to fill that gap by exploring the influence of generator temperature on fluid flow behavior, condensation, and evaporation processes, with the aim of providing a comprehensive understanding of both the WSM and DSM.

Subsequently, the effect of generator temperature on the ER was investigated in each of the aforementioned models.

2. Governing equation and numerical method

In present study, the flow in the ejector is governed by the steady-state, compressible, and axisymmetric form of the fluid flow conservation equations. The single-fluid approach and Eulerian perspective *et al*., 2020) were used to simulate the Navier-Stokes equations as well as the humidity equations and droplet number. This viewpoint considers the mixed phase equations for the liquid and vapor phases (Aliabadi, Lakzian, Khazaei, *et al*., 2020).

2.1. The description of DSM equations

In this model, only the vapor phase is modeled and the phase change and liquid phase growth are omitted. The continuity equation, momentum equation and energy equation are as follows (Aliabadi, Lakzian, Jahangiri, *et al*., 2020; Aliabadi, Lakzian, Khazaei, *et al*., 2020; Aliabadi & Bahiraei, 2021).

$$\frac{\partial \rho}{\partial t}+\frac{\partial(\rho u_j)}{\partial x_j}=0 \tag{1}$$

$$\frac{\partial(\rho u_i)}{\partial t}+\frac{\partial(\rho u_j u_i+P\delta_{ji})}{\partial x_j}-\frac{\partial \tau_{ji}}{\partial x_j}=0 \tag{2}$$

$$\frac{\partial(\rho E)}{\partial t}+\frac{\partial(\rho u_j H)}{\partial x_j}+\frac{\partial(q_j-u\tau_{ji})}{\partial x_j}=0 \tag{3}$$

P is pressure, ρ is density, and h is enthalpy.

2.2. The description of WSM equations

In this method, the phase change impact is considered to the all equations and two-phase flow is simulated. In other words, the humidity equations and number of drops are solved simultaneously with the flow equations. The humidity equation and number of drops equation are as follows (Hosseinizadeh *et al*., 2023).

$$\frac{\partial(\rho y)}{\partial t}+\frac{\partial(\rho u_j y)}{\partial x_j}=\Gamma_1+\Gamma_2 \tag{4}$$

$$\frac{\partial(\rho n)}{\partial t}+\frac{\partial(\rho u_j n)}{\partial x_j}=\rho J \tag{5}$$

y is LMF and n is number of droplets. Γ_1 and Γ_2 are used to define change of phase for droplet growth (Γ_2) and nucleation (Γ_1) (Wróblewski *et al*., 2009).

$$\Gamma_1=\frac{4}{3}\pi\rho_l\rho r^{*3}J \tag{6}$$

$$\Gamma_2=4\pi\rho_l\rho n r^2\frac{dr}{dt} \tag{7}$$

The subscripts v and l refer to the vapor phase and liquid phase. r is droplet radius and $\frac{dr}{dt}$ is droplets growth. Nucleation and droplet growth are major processes in the condensation phenomenon. The homogeneous nucleation model is used in present study. Condensation takes place in this type of nucleation without the presence of surfaces or impurities. The nucleation phenomenon is the development of new droplets that have a critical size. The non-isothermal non-equilibrium condensation theory can be used to compute the rate of droplet production per unit volume due to spontaneous condensation. The equation of classical nucleation and corrections of Kantrowitz are given by (Aliabadi, Jahangiri, *et al*., 2020; Talebi Somesaraee *et al*., 2018).

$$J_{class}=q_c\sqrt{\frac{2\sigma_r}{\pi}}m_m^{-3/2}\frac{\rho_v}{\rho_l}exp\left(\frac{-4\pi r^{*2}\sigma_r}{3K_bT_v}\right) \tag{8}$$

$$J=\frac{1}{1+\emptyset}J_{class} \tag{9}$$

where, q_c indicates condensation coefficient, M_m shows the mass of a water molecule, r^* demonstrates the Kelvin-Helmholtz critical droplet radius, σ is surface tension, and k_b is Boltzmann constant (Faghih Aliabadi *et al*., 2017). $\emptyset$ is the temperature correction coefficient (Dolatabadi *et al*., 2023).

$$\emptyset=2\frac{(\gamma-1)}{(\gamma+1)}\frac{h_{lv}}{RT_v}\left(\frac{h_{lv}}{RT_v}-\frac{1}{2}\right) \tag{10}$$

$$r^*=\frac{2\sigma}{\rho_l RT\ln P/P_s} \tag{11}$$

P_s is saturation pressure and R is gas constant. The droplet growth equation is one of the chief relations in modeling the condensation flow of wet steam. The below droplet growth equation used in present study is one of the most applied droplet growth formulas (Jahangiri *et al*., 2023):

$$\frac{dr}{dt}=\frac{1}{\rho_l}\frac{\lambda_v}{(1+3.18Kn)}\frac{r-r^*}{r^2}\frac{T_s-T_v}{h_v-h_l} \tag{12}$$

2.3. Entrainment ratio

The major parameter for an ejector can be explained as the ER. The ER is calculated as (Wang *et al*., 2022):

Table 1
Geometric details of the steam ejector (GFL Al-Doori, 2013)

Geometric parameters	Size (mm)
Inlet diameter of primary nozzle inlet diameter	10
Throat diameter of primary nozzle	3.2
Outlet diameter of primary nozzle	13.6
Divergent length of primary nozzle	59.5
Inlet diameter of mixing chamber	37
Length of mixing chamber	155
Diameter of constant area	25.4
Length of constant area	75
Length of subsonic diffuser	210
Outlet diameter of subsonic diffuser	50

Table 2
Pressure and temperature for the steam ejector boundaries.

Stream	Temperature (K)	Pressure (kPa)
Primary	403	270
Secondary	287	1.6
Discharge	-	4.2

Table 3
Grid independence study.

Grid cells	Mass flow rate [kg/s]		
	Motive	Suction	ER
11000	0.00339	0.00115	0.339
57000	0.00333	0.00125	0.376
89000	0.00333	0.00122	0.377

Table 4
Validation

	Experiment	Present study	Mazelli (Mazzelli *et al.*, 2018)
Entrainment ratio	0.33	0.376	0.377

$$ER = \frac{\dot{m}_s}{\dot{m}_p} \quad (12)$$

Where mass flow rates of the primary and secondary are depicted by $\dot{m}_p$ and $\dot{m}_s$, respectively.

2.4. *Numerical schemes*

The available CFD solver ANSYS FLUENT 20 software was applied to carry out the simulations. C programming codes were written to simulate additional transport equations of the liquid fractions and droplets number. The *k-ω* SST turbulence model was employed for the RANS method (Wen *et al*., 2020; Yang *et al*., 2019). The control volume method and the density-based method were chosen to solve the steady and axisymmetric equations. The scheme of the second-order upwind method and central difference method was used to discretize the convection and diffusion terms. The convergence criteria are considered satisfied when the calculation residuals are less than 10-6 for all parameters.

2.5. *Mesh study and validation*

In this research, an ejector is used to investigate the effect of the generator temperature designed by (GFL Al-Doori, 2013) to start a refrigeration cycle. The geometric structure of this ejector is shown in Table 1. The length of mixing chamber and NXP are equal to 155 mm and 6 mm. The ejector boundary conditions are shown in Table 2. The primary flow temperature is 403 K, the secondary flow temperature is 287 K and the discharge pressure is 4.2 kPa. Table 3 shows the computing grid-independence of the solution. The number of cells 11000, 57000 and 89000 are considered for present study. It can be seen that between the number of cells 57000 and 89000, there is a slight difference in ER (less than 0.02%). 57000 cells are used to reduce the computational cost. Fig. 1 shows the computational domain. Table 4 shows the validation of the present numerical solution. The ER calculated in this research is equal to 0.376. In their study, (Mazzelli *et al*., 2018) calculated the ER to be 0.377, and the experimental data is 0.33. This shows that the present numerical solution can well predict the value of the ER in the ejector.

3. Result and discussion

In recent times, the steam ERC has gained considerable attention due to its numerous advantages. Despite having a low COP, researchers have conducted several studies to address this limitation. The present study aims to illustrate the influence

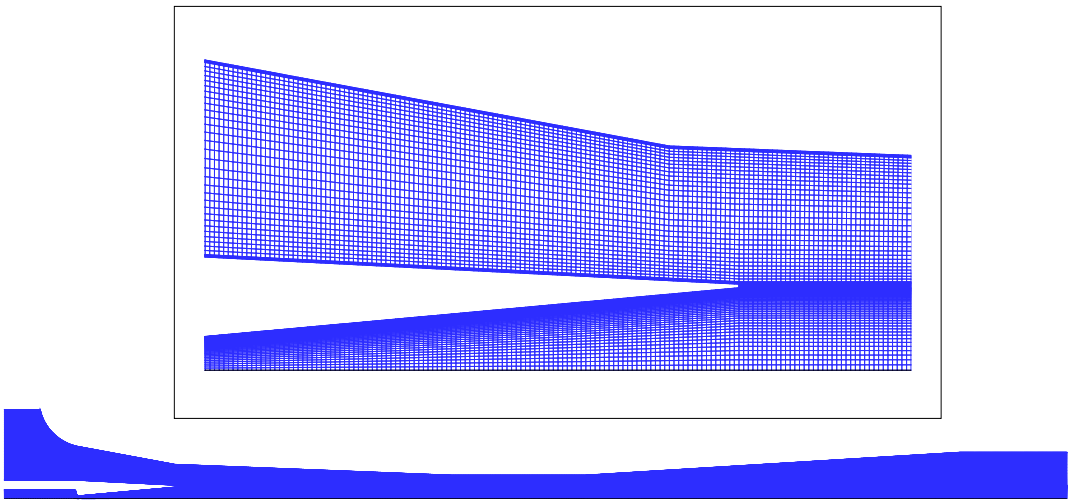

Fig. 1. Computational grids of ejector

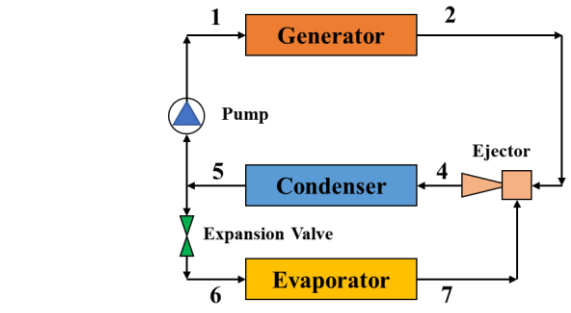

(a)

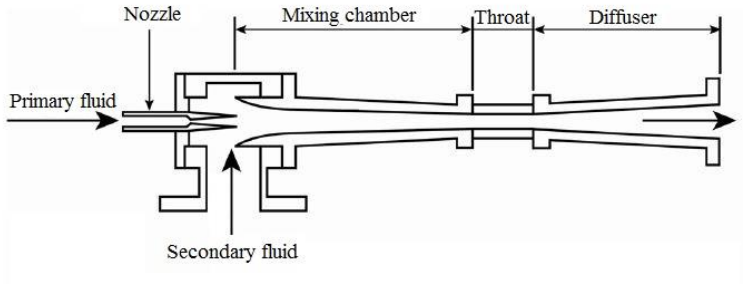

(b)

Fig. 2. Ejector refrigeration cycle a) Component of system b) Ejector structure

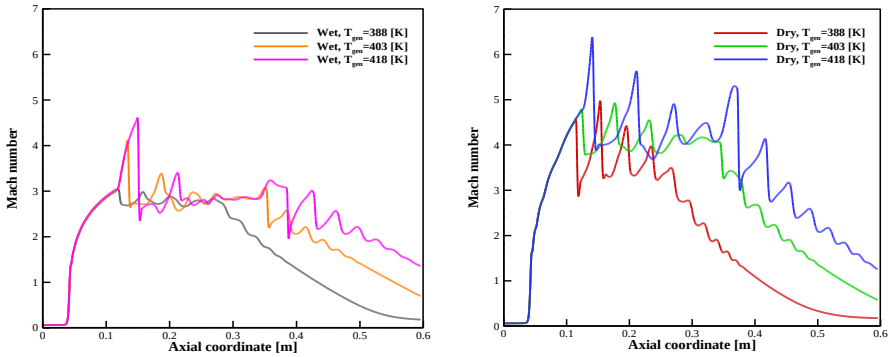

a) Mach number profiles at the central line of the steam ejector

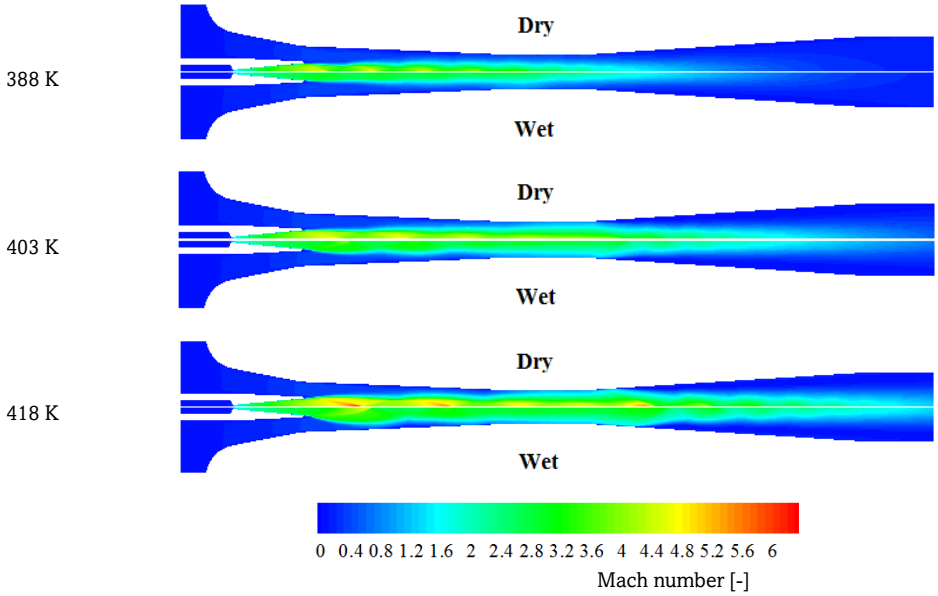

b) Mach number contours along the steam ejector

Fig. 3. Effect of generator temperature on Mach number distribution in steam ejector for Wet steam model and Dry steam model

of generator temperature rise on ejector efficiency and compare the simulation results between the WSM and the DSM. In the refrigeration cycle, the generator operates at saturation temperature and produces saturated steam. This steam enters the ejector, where it combines with the flow drawn from the evaporator. The combined flow then exits the ejector and enters

the condenser (G. Zhang, Wang, Pourranjbar, *et al.*, 2022). To assess the impact of generator temperature, a temperature range of 388 K to 418 K is considered. The present study also investigates the effects of WSM and DSM within this temperature range. Notably, WSM and DSM differ significantly in their treatment of phase change. WSM incorporates phase change effects into its calculations, accounting for the heat transfer associated with phase change. By considering condensation and evaporation processes in the simulation, it becomes possible to observe the effects of phase change on aerodynamic shocks, mixing rate, and entropy production. Figure 2 illustrates the ERC as visualized in the study.

3.1. Investigating the impact of generator temperature rise on flow behavior in WSM and DSM

This section focuses on examining the influence of increasing generator temperature on the Mach number and temperature within the system. Figure 3 showcases the effect of generator temperature on the Mach number for both the WSM and the DSM. Specifically, temperatures of 388 K, 403 K, and 418 K were considered to investigate this impact. As the steam enters the ejector with high pressure, it undergoes expansion and reaches the supersonic state within the primary nozzle, resulting in an increase in the Mach number. The steam continues to expand further, reaching its maximum velocity at the exit of the primary nozzle and the start of the mixing chamber, where the Mach number reaches its peak. In this region, there is a significant drop in pressure, creating a low-pressure zone that draws in the secondary flow into the ejector. Subsequently, the Mach number decreases due to the occurrence of aerodynamic shocks within the system *et al.*, 2019).

According to Fig. 2, the difference in Mach number between WSM and DSM is significant. The Mach number in the DSM is higher than that of the WSM, and the intensity of the aerodynamic shocks in the DSM is greater than that of the WSM (Yang *et al.*, 2019). Also, as the generator temperature increases, the Mach number at the ejector output increases. At a temperature of 418 K, the maximum Mach number for the dry steam model is 6.38 at x=0.14 m and for the wet steam model is 4.61 at x=0.149 m. After shock, the Mach number for DSM and WSM decreases to 3.88 and 2.35, respectively. Mach number at the outlet for DSM and WSM is 1.26 and 1.35 respectively. Fig. 4 shows the effect of generator temperature on temperature distribution for WSM and DSM. The static temperatures of 388 K, 403 K and 418 K are considered in present study. It is quite significant the difference between the DSM and the WSM. A very sharp drop in temperature is seen in the DSM, and the temperature in many places is below 273 K; and it becomes less than 100 K near x=0.11 m. But the temperature becomes less than 273 K in the WSM due to the strong expansion. Then, with the occurrence of aerodynamic shocks, the temperature rises above 273 K. Phase change and transfer of latent heat to flow prevents extreme temperature changes in WSM. A temperature rise is observed in the WSM near x=0.04 m, which is caused by condensation shock. The temperature increases slowly at a temperature of 388 K and near x=0.52 m. Single-phase flow is the reason for this rise in temperature, which is explained in the next part. The minimum temperature decreases in the WSM as the generator temperature increases, and the intensity of aerodynamic shocks increases. According to reference (Mazzelli *et al.*, 2018), it is possible for ice nucleation to occur at a temperature below 273 K, but this phenomenon may not occur due to insufficient time and a sudden rise in temperature.

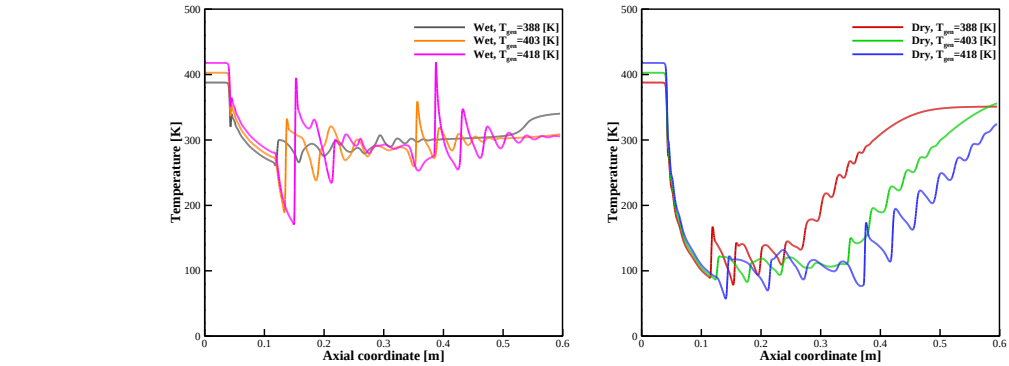

a) Temperature profiles at the central line of the steam ejector

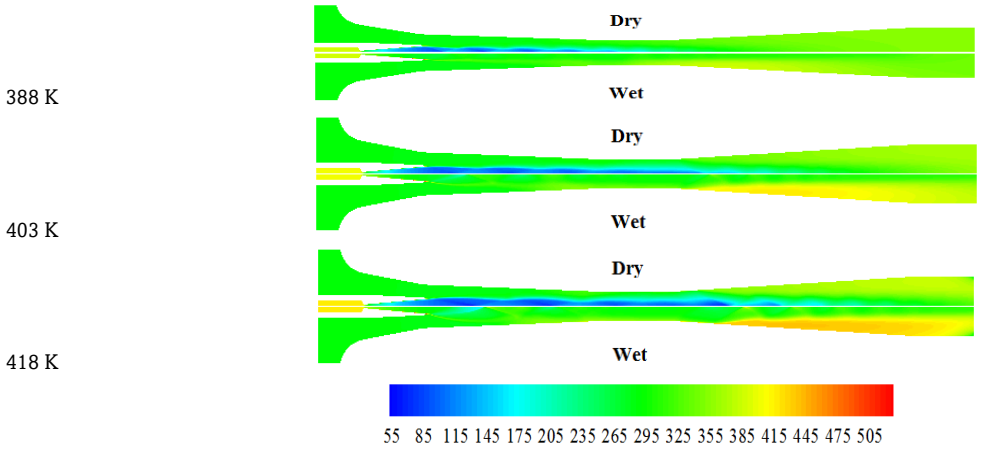

b) Temperature contours along the steam ejector

Fig. 4. Effect of generator temperature on temperature distribution in steam ejector for Wet steam model and Dry steam model

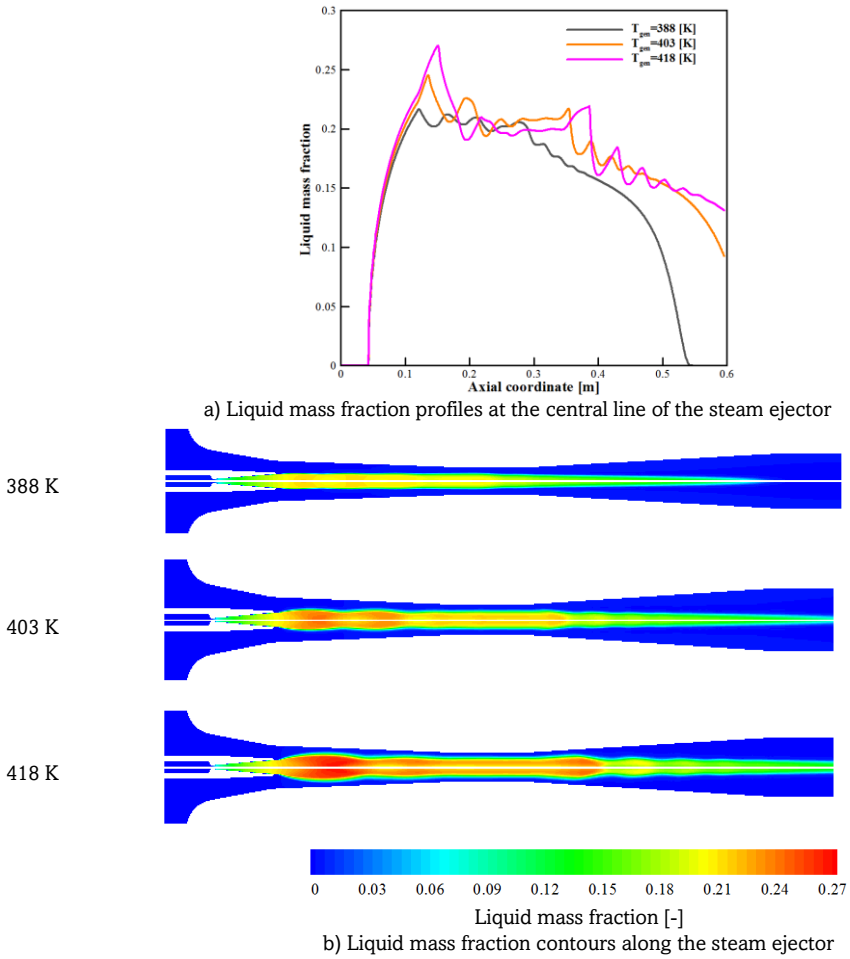

a) Liquid mass fraction profiles at the central line of the steam ejector

b) Liquid mass fraction contours along the steam ejector

Fig. 5. Effect of generator temperature on liquid mass fraction distribution in steam ejector for Wet steam model

3.2. Investigating the impact of temperature rise on the liquid phase in the WSM

One of the most important parameters of the WSM is the LMF, which shows the amount of the liquid phase at each location. By increasing the LMF, we can see that condensation has occurred, and by decreasing the LMF, we can see that evaporation has occurred (Aliabadi & Bahiraei, 2021). Zero mass fraction of the liquid means that the flow becomes single-phase. The impact of generator temperature on LMF is shown in Fig. 5. As the generator temperature increases, more phase of liquid is seen in the ejector, and the maximum LMF in the ejector increases. The maximum LMF for each of the temperatures 388 K, 403 K and 418 K is equal to 0.211, 0.245 and 0.270, respectively. At a temperature of 388 K and near x=0.52 m, the LMF becomes zero, and the flow becomes single-phase. The fluctuations seen in the LMF are caused by aerodynamic shocks. The most important feature of the WSM is the visibility of the liquid phase, and the liquid phase has a significant effect on the flow behavior.

3.3. The generator temperature rise impact on performance of ejector considering WSM and DSM

In this section, the influence of increasing generator temperature on the mass flow rates of the primary and secondary flows, as well as the ER, is explored. As previously mentioned, the WSM and the DSM differ significantly in the temperature and Mach number. It is crucial to determine the flow rates of both the secondary flow and the motive flow to accurately assess the ejector's performance. Figure 6 presents the impact of generator temperature rise on the primary and secondary mass flow rates, as well as the ER, for both the DSM and WSM. The generator temperature range considered in ranges from 388 K to 418 K. As the temperature of the generator increases, the motive flow rate for both models also increases, with no significant difference observed between the WSM and the DSM. Because the temperature distribution and Mach number distribution in the converging part of the primary nozzle (x<0.05 m) is the same for both models.

The secondary flow rate does not exhibit a consistent trend, and except for the temperature of 388 K, the mass flow rate of the secondary flow is generally higher in the DSM compared to the WSM. Temperature distribution and Mach number distribution for both models at the exit of the primary nozzle have different values. For this reason, the secondary flow rate is different in both models. It should be noted that the low-pressure area at the end of the primary nozzle causes the flow to be sucked into the ejector. Latent heat resulting from condensation and evaporation is the reason for the difference between the WSM and the WDM.

As the temperature of the generator increases, the ER decreases. Moreover, the ER of the DSM (excluding the temperature of 388 K) tends to be higher than that of the WSM. For instance, at a temperature of 388 K, the ER for the WSM and DSM is 0.59 and 0.55, respectively. As the temperature increases from 388 K to 418 K, the ER for the WSM and DSM decreases to 0.19 and 0.23, respectively. The decrease in the ER can be attributed to two factors.

- Reducing suction mass flow rate

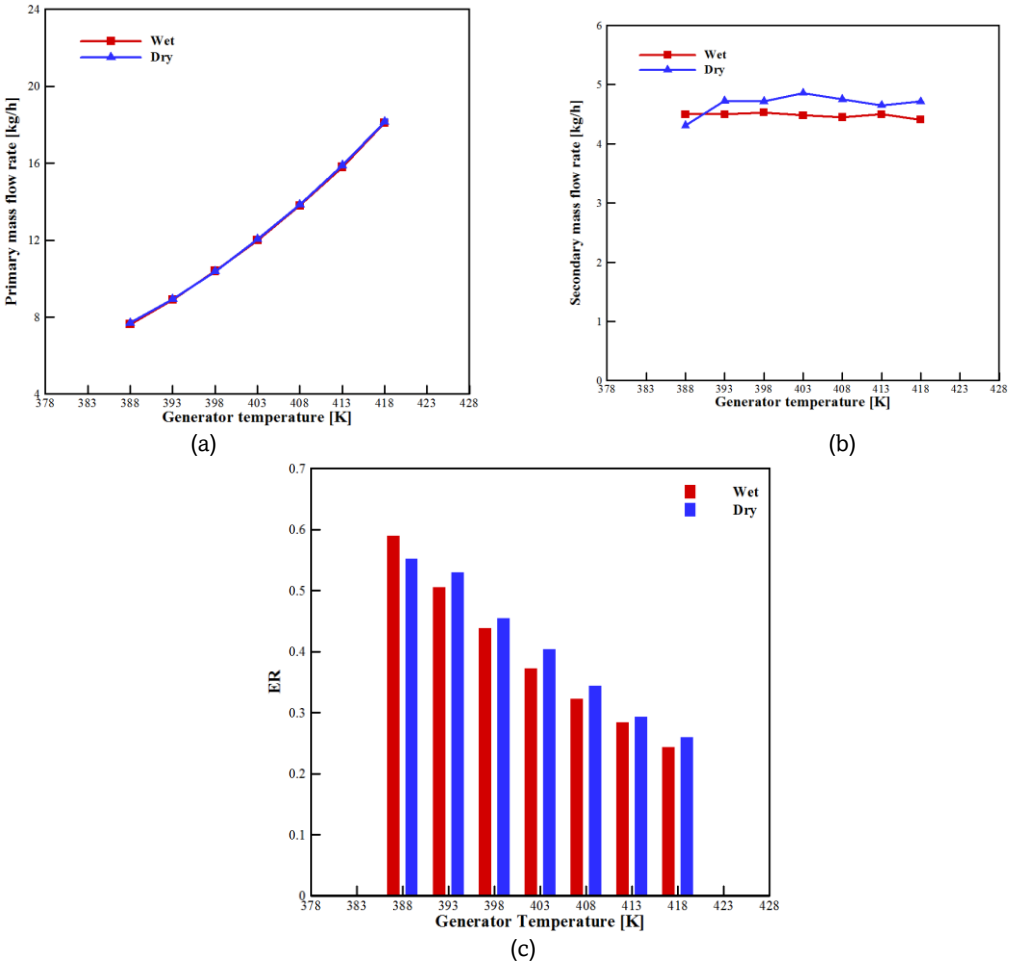

Fig. 6. Effect of generator temperature on a) Primary mass flow rate b) Secondary mass flow rate c) Entrainment ratio

- Increasing the motive mass flow rate

With an increase in the temperature of the generator, the pressure within the system rises, leading to an expected increase in the primary mass flow rate. Conversely, the changes in the mass flow rate of the secondary flow are relatively minimal. As a result, it can be concluded that the primary mass flow rate increase is the primary factor contributing to the decrease in the ER.

3.3. The effect of generator temperature rise on entropy production considering WSM and DSM

In this section, the assessment of entropy production within the ejector is conducted. The study focuses on several crucial factors that contribute to entropy production, including flow mixing, friction, aerodynamic shocks (such as oblique shocks and normal shocks), and phase change (specifically, the condensation and evaporation processes) (Jahangiri *et al.*, 2023).

Figure 7 illustrates the impact of increasing generator temperature on entropy production for both the DSM and WSM. The results demonstrate that the entropy produced in the WSM is lower compared to the DSM. As the generator temperature increases, there is a corresponding increase in entropy production. Furthermore, as the generator temperature rises, the difference in entropy production between the DSM and the WSM decreases. For instance, at a temperature of 388 K, the production entropy is 2.2 W/K for the WSM and 3.3 W/K for the DSM. As the temperature increases from 388 K to 418 K, the production entropy for the WSM reaches 10.7 W/K, while for the DSM, it reaches 10.3 W/K. Figure 3 depicts that as the generator temperature increases, the intensity of aerodynamic shocks becomes more pronounced. Aerodynamic shocks are inherently irreversible processes that contribute to entropy production. Therefore, with the intensification of these shocks, an increase in production entropy is expected. As the temperature of the generator increases, the losses due to

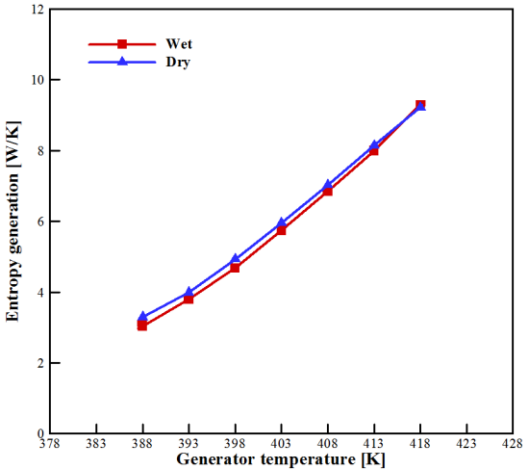

Fig. 7. Entropy generation in steam ejector

aerodynamic shocks increase so much that the entropy production in the WSM and the DSM are close together.

4. Conclusion

Present study examines the flow structure of a ejector utilizing both the WSM and DSM. The primary focus is to assess the impact of increasing the generator temperature on various aspects, including the aerodynamic shock pattern, mixing rate, production entropy, temperature distribution, and Mach number. The WSM takes into account condensation and evaporation processes, while the DSM considers only the vapor phase flow. With an increase in generator temperature, both the WSM and DSM exhibit an amplification in Mach number distribution and shock intensity. At a temperature of 418 K, the maximum Mach number recorded in the DSM and WSM is 6.38 and 4.81, respectively.

A noticeable distinction in temperature distribution is observed between the DSM and the WSM, with the DSM exhibiting temperatures below 100 K. With an increase in generator temperature, the ER decreases in both models, and except for the temperature of 388 K, the WSM consistently displays a lower ER compared to the DSM. Moreover, as the generator temperature rises, the production entropy increases in both models, with the WSM generally exhibiting lower production entropy than the DSM. As the static temperature of the generator increases, a larger proportion of liquid phase is generated within the ejector, leading to a decrease in entropy difference between the two models. Present study contributes to a better comprehension of flow behavior within the ejector.

Reference

Abbady, K., Al-Mutawa, N., & Almutairi, A. (2023). The performance analysis of a variable geometry ejector utilizing CFD and artificial neural network. *Energy Conversion and Management*, *291*, 117318. https://doi.org/10.1016/j.enconman.2023.117318

Alami, A. H., Alrashid, R., Mdallal, A., Yasin, A., Ayoub, M., Alasad, S., Aljaghoub, H., Alashkar, A., Abdelkareem, M. A., & Olabi, A. G. (2023). Expansion cooling prospects for large scale applications. *International Journal of Thermofluids*, 100437. https://doi.org/10.1016/j.ijft.2023.100437

Aliabadi, M. A. F., & Bahiraei, M. (2021). Effect of water nano-droplet injection on steam ejector performance based on non-equilibrium spontaneous condensation: A droplet number study. *Applied Thermal Engineering*, *184*, 116236. https://doi.org/10.1016/j.applthermaleng.2020.116236

Aliabadi, M. A. F., Jahangiri, A., Khazaee, I., & Lakzian, E. (2020). Investigating the effect of water nano-droplets injection into the convergent-divergent nozzle inlet on the wet steam flow using entropy generation analysis. *International Journal of Thermal Sciences*, *149*, 106181. https://doi.org/10.1016/j.ijthermalsci.2019.106181

Aliabadi, M. A. F., Lakzian, E., Jahangiri, A., & Khazaei, I. (2020). Numerical investigation of effects polydispersed droplets on the erosion rate and condensation loss in the wet steam flow in the turbine blade cascade. *Applied Thermal Engineering*, *164*, 114478. https://doi.org/10.1016/j.applthermaleng.2019.114478

Aliabadi, M. A. F., Lakzian, E., Khazaei, I., & Jahangiri, A. (2020). A comprehensive investigation of finding the best location for hot steam injection into the wet steam turbine blade cascade. *Energy*, *190*, 116397. https://doi.org/10.1016/j.energy.2019.116397

Aliabadi, M. A. F., Zhang, G., Dykas, S., & Li, H. (2021). Control of two-phase heat transfer and condensation loss in turbine blade cascade by injection water droplets. *Applied Thermal Engineering*, *186*, 116541. https://doi.org/10.1016/j.applthermaleng.2020.116541

Banasiak, K., Palacz, M., Hafner, A., Buliński, Z., Smołka, J., Nowak, A. J., & Fic, A. (2014). A CFD-based investigation of the energy performance of two-phase R744 ejectors to recover the expansion work in refrigeration systems: An irreversibility analysis. *International Journal of Refrigeration*, *40*, 328–337. https://doi.org/10.1016/j.ijrefrig.2013.12.002

Besagni, G., & Inzoli, F. (2017). Computational fluid-dynamics modeling of supersonic ejectors: Screening of turbulence modeling approaches. *Applied Thermal Engineering*, *117*, 122–144. https://doi.org/10.1016/j.applthermaleng.2017.02.011

Bordbar, B., Khosravi, A., Abdollahi, F., Hashemifard, S. A., & Karagöz, S. (2023). An insight into environmental footprints of emerging air-conditioning systems towards sustainable cities. *Sustainable Cities and Society*, *98*, 104830. https://doi.org/10.1016/j.scs.2023.104830

Chen, R., & Weng, G. (2023). Sustainable Energy Resources for Driving Methane Conversion. *Advanced Energy Materials*, *13*(36), 2301734. https://doi.org/10.1002/aenm.202301734

Deng, J., Jiang, P., Lu, T., & Lu, W. (2007). Particular characteristics of transcritical CO2 refrigeration cycle with an ejector. *Applied Thermal Engineering*, *27*(2–3), 381–388. https://doi.org/10.1016/j.applthermaleng.2006.07.016

Dokandari, D. A., Hagh, A. S., & Mahmoudi, S. M. S. (2014). Thermodynamic investigation and optimization of novel ejector-expansion CO2/NH3 cascade refrigeration cycles (novel CO2/NH3 cycle). *International Journal of Refrigeration*, *46*, 26–36. https://doi.org/10.1016/j.ijrefrig.2014.07.012

Dolatabadi, A. M., Pour, M. S., Ajarostaghi, S. S. M., Poncet, S., & Hulme-Smith, C. (2023). Last stage stator blade profile improvement for a steam turbine under a non-equilibrium condensation condition: A CFD and cost-saving approach. *Alexandria Engineering Journal*, *73*, 27–46. https://doi.org/10.1016/j.aej.2023.04.011

Elsheniti, M. B., AlRabiah, A., Al-Ansary, H., Almutairi, Z., Orfi, J., & El-Leathy, A. (2023). Performance Assessment of an Ice-Production Hybrid Solar CPV/T System Combining Both Adsorption and Vapor-Compression Refrigeration Systems. *Sustainability*, *15*(4), 3711. https://doi.org/10.3390/su15043711

Faghih Aliabadi, M. A., & Mahpeykar, M. R. (2017). Comparison between polydispersed and monodispersed models on condensing water-vapor flow in a supersonic convergent-divergent nozzle. *Modares Mechanical Engineering*, *17*(3), 19–30. https://mme.modares.ac.ir/article-15-9609-en.html

GFL Al-Doori. (2013). Investigation of refrigeration system steam ejector performance through experiments and computational simulations. PhD Thesis Doctor of Philosophy. University of Southern Queensland. https://research.usq.edu.au/item/q1zv6/investigation-of-refrigeration-system-steam-ejector-performance-through-experiments-and-computational-simulations

Haghparast, P., Sorin, M. V, & Nesreddine, H. (2018). The impact of internal ejector working characteristics and geometry on the performance of a refrigeration cycle. *Energy*, *162*, 728–743. https://doi.org/10.1016/j.energy.2018.08.017

Hosseinizadeh, S. E., Ghamati, E., Jahangiri, A., Majidi, S., Khazaee, I., & Aliabadi, M. A. F. (2023). Reduction of water droplets effects in steam turbine blade using Multi-objective optimization of hot steam injection. *International Journal of Thermal Sciences*, *187*, 108155. https://doi.org/10.1016/j.ijthermalsci.2023.108155

Hui, X., Ma, Y., & Deng, X. (2023). Numerical simulation on effects of augmentation in temperature of inlet steam on wet steam flow in supersonic nozzle: energy and exergy analysis. *Multiscale and Multidisciplinary Modeling, Experiments and Design*, 1–10. https://doi.org/10.1007/s41939-023-00164-x

Jahangiri, A., Aliabadi, M. A. F., Pourranjbar, D., Mottahedi, H. R., Gharebaei, H., & Ghamati, E. (2023). A comprehensive investigation of non-condensable gas and condenser temperature effects on power plant ejector performance by considering condensation flow regime. *Thermal Science and Engineering Progress*, *45*, 102128. https://doi.org/10.1016/j.tsep.2023.102128

Kulkarni, S., Chavali, S., & Dikshit, S. (2023). A review on analysis of Vapour Compression Refrigeration System (VCRS) for its performance using different ecofriendly refrigerants and nanofluids. *Materials Today: Proceedings*, *72*, 878–883. https://doi.org/10.1016/j.matpr.2022.09.085

Lee, T.-S., Liu, C.-H., & Chen, T.-W. (2006). Thermodynamic analysis of optimal condensing temperature of cascade-condenser in CO2/NH3 cascade refrigeration systems. *International Journal of Refrigeration*, *29*(7), 1100–1108. https://doi.org/10.1016/j.ijrefrig.2006.03.003

Liang, Y., Ye, K., Zhu, Y., & Lu, J. (2023). Thermodynamic analysis of two-stage and dual-temperature ejector refrigeration cycles driven by the waste heat of exhaust gas. *Energy*, *278*, 127862. https://doi.org/10.1016/j.energy.2023.127862

Ma, D., Sun, Y., Ma, S., Li, G., Zhou, Z., & Ma, H. (2024). Study on the working medium of high temperature heat pump suitable for industrial waste heat recovery. *Applied Thermal Engineering*, *236*, 121642. https://doi.org/10.1016/j.applthermaleng.2023.121642

Marenco-Porto, C. A., Fierro, J. J., Nieto-Londoño, C., Lopera, L., Escudero-Atehortua, A., Giraldo, M., & Jouhara, H. (2023). Potential savings in the cement industry using waste heat recovery technologies. *Energy*, 127810. https://doi.org/10.1016/j.energy.2023.127810

Mazzelli, F., Giacomelli, F., & Milazzo, A. (2018). CFD modeling of condensing steam ejectors: Comparison with an experimental test-case. *International Journal of Thermal Sciences*, *127*, 7–18. https://doi.org/10.1016/j.ijthermalsci.2018.01.012

Mazzelli, F., Little, A. B., Garimella, S., & Bartosiewicz, Y. (2015). Computational and experimental analysis of supersonic air ejector: Turbulence modeling and assessment of 3D effects. *International Journal of Heat and Fluid Flow*, *56*, 305–316. https://doi.org/10.1016/j.ijheatfluidflow.2015.08.003

Mungyeko Bisulandu, B.-J. R., Mansouri, R., & Ilinca, A. (2023). Diffusion absorption refrigeration systems: An overview of thermal mechanisms and models. *Energies*, *16*(9), 3610. https://doi.org/10.3390/en16093610

Prabakaran, R., Lal, D. M., & Kim, S. C. (2023). A state of art review on future low global warming potential refrigerants and performance augmentation methods for vapour compression based mobile air conditioning system. *Journal of Thermal Analysis and Calorimetry*, *148*(2), 417–449. https://doi.org/10.1007/s10973-022-11485-3

Sarkar, J., & Bhattacharyya, S. (2010). Thermodynamic analyses and optimization of a transcritical N2O refrigeration cycle. *International Journal of Refrigeration*, *33*(1), 33–40. https://doi.org/10.1016/j.ijrefrig.2009.09.012

Sharif, M. Z., Azmi, W. H., Ghazali, M. F., Samykano, M., & Ali, H. M. (2023). Performance improvement strategies of R1234yf in vapor compression refrigeration system as a R134a replacement: A review. *Journal of the Taiwan Institute of Chemical Engineers*, 105032. https://doi.org/10.1016/j.jtice.2023.105032

Sierra-Pallares, J., Del Valle, J. G., Carrascal, P. G., & Ruiz, F. C. (2016). A computational study about the types of entropy generation in three different R134a ejector mixing chambers. *International Journal of Refrigeration*, *63*, 199–213. https://doi.org/10.1016/j.ijrefrig.2015.11.007

Talebi Somesaraee, M., Amiri Rad, E., & Mahpeykar, M. R. (2018). Analytical investigation of simultaneous effects of convergent section heating of Laval nozzle, steam inlet condition, and nozzle geometry on condensation shock. *Journal of Thermal Analysis and Calorimetry*, *133*, 1023–1039. https://doi.org/10.1007/s10973-018-7126-x

Tang, Y., Liu, Z., Li, Y., Wu, H., Zhang, X., & Yang, N. (2019). Visualization experimental study of the condensing flow regime in the transonic mixing process of desalination-oriented steam ejector. *Energy Conversion and Management*, *197*, 111849. https://doi.org/10.1016/j.enconman.2019.111849

Wang, C., & Wang, L. (2022). Investigation of Fluid Characteristic and Performance of an Ejector by a Wet Steam Model. *Entropy*, *25*(1), 85. https://doi.org/10.3390/e25010085

Wen, C., Ding, H., & Yang, Y. (2020). Performance of steam ejector with nonequilibrium condensation for multi-effect distillation with thermal vapour compression (MED-TVC) seawater desalination system. *Desalination*, *489*, 114531. https://doi.org/10.1016/j.desal.2020.114531

Wróblewski, W., Dykas, S., & Gepert, A. (2009). Steam condensing flow modeling in turbine channels. *International Journal of Multiphase Flow*, *35*(6), 498–506. https://doi.org/10.1016/j.ijmultiphaseflow.2009.02.020

Yang, Y., Zhu, X., Yan, Y., Ding, H., & Wen, C. (2019). Performance of supersonic steam ejectors considering the nonequilibrium condensation phenomenon for efficient energy utilisation. *Applied Energy*, *242*, 157–167. https://doi.org/10.1016/j.apenergy.2019.03.023

Yari, M., & Mahmoudi, S. M. S. (2011). Thermodynamic analysis and optimization of novel ejector-expansion TRCC (transcritical CO2) cascade refrigeration cycles (Novel transcritical CO2 cycle). *Energy*, *36*(12), 6839–6850. https://doi.org/10.1016/j.energy.2011.10.012

Yıldız, G., Gürel, A. E., Ceylan, İ., Ergün, A., Karaağaç, M. O., & Ağbulut, Ü. (2023). Thermodynamic analyses of a novel hybrid photovoltaic-thermal (PV/T) module assisted vapor compression refrigeration system. *Journal of Building Engineering*, *64*, 105621. https://doi.org/10.1016/j.jobe.2022.105621

Zhang, G., Wang, X., Dykas, S., & Aliabadi, M. A. F. (2022). Reduction entropy generation and condensation by NaCl particle injection in wet steam supersonic nozzle. *International Journal of Thermal Sciences*, *171*, 107207. https://doi.org/10.1016/j.ijthermalsci.2021.107207

Zhang, G., Wang, X., Pourranjbar, D., Dykas, S., Li, H., & Chen, J. (2022). The comprehensive analysis of the relationship between the latent heat, entrainment ratio, and ejector performance under different superheating degree conditions considering the non-equilibrium condensation. *Applied Thermal Engineering*, *200*, 117701. https://doi.org/10.1016/j.applthermaleng.2021.117701

Zhang, G., Zhang, X., Wang, D., Jin, Z., & Qin, X. (2019). Performance evaluation and operation optimization of the steam ejector based on modified model. *Applied Thermal Engineering*, *163*, 114388. https://doi.org/10.1016/j.applthermaleng.2019.114388

Zhang, H., Pan, X., Chen, J., & Xie, J. (2023). Energy, exergy, economic and environmental analyses of a cascade absorption-compression refrigeration system using two-stage compression with complete intercooling. *Applied Thermal Engineering*, *225*, 120185. https://doi.org/10.1016/j.applthermaleng.2023.120185

Zhang, Z., Fu, S., & Marefati, M. (2023). A waste heat and liquefied natural gas cold energy recovery-based hybrid energy cycle: An effort to achieve superior thermodynamic and environmental performances. *Process Safety and Environmental Protection*, *177*, 322–339. https://doi.org/10.1016/j.psep.2023.06.085